ELSEVIER

Polymer Vol. 37 No. 13, pp. 2801–2809, 1996

0032-3861/96/$15.00 + 0.00

Microporous polymeric materials by polymerization of microemulsions containing different alkyl chain lengths of cationic surfactants

T. H. Chieng*, L. M. Gan and C. H. Chew
Department of Chemistry, National University of Singapore, Kent Ridge, Singapore 119260

and S. C. Ng
Department of Physics, National University of Singapore, Kent Ridge, Singapore 119260

and K. L. Pey
Institute of Microelectronics, National University of Singapore, 11 Science Park Road, Science Park II, Singapore 117685
(Received 10 October 1995)

Microemulsion systems formulated with methyl methacrylate, 2-hydroxyethyl methacrylate, cross-linking agent, ethylene glycol dimethacrylate (EGDMA) and water using cationic surfactants of *n*-alkyl trimethyl ammonium bromide with alkyl chain lengths varying from C12 to C16 have been investigated. Photoinitiated polymerization was carried out only for bicontinuous microemulsion samples to form microporous polymeric materials. The opacity of the resulting polymeric materials decreased with the use of shorter alkyl chain lengths of the cationic surfactants. In addition, the morphology of the microporous polymeric solids as observed by Field Emission Scanning Electron Microscope shows a drastic change from worm-like, oval-shaped to globular structures on decreasing the alkyl chain length of the surfactant at a particular concentration. These polymeric materials possessed open-cell structures. Their pore sizes were smaller and their pore volume distributions were narrower for polymer samples using shorter alkyl chain-length surfactants. This study shows the feasibility of controlling the microstructures and pore dimensions of the polymeric materials prepared by polymerization of bicontinuous microemulsions containing different alkyl chain lengths of cationic surfactants. Copyright © 1996 Elsevier Science Ltd.

(Keywords: bicontinuous microemulsions; microporous polymeric materials; microstructures)

INTRODUCTION

Microemulsions, in contrast to emulsions, are thermodynamically stable, transparent isotropic liquid consisting of aqueous and oil phases stabilized by a surfactant or a combination of surfactant and cosurfactant. Short-chain alcohols are commonly used as cosurfactant. There are three types of microemulsions, namely water-in-oil (w/o) microemulsion, oil-in-water (o/w) microemulsion and bicontinuous microemulsion. The former two types have been widely studied for the preparation of nanosize polymer latexes[1–5]. The bicontinuous microemulsion characterized by low interfacial tension (10^{-6} Nm^{-1}) has also been employed to prepare a higher content of polymer latexes with a lower amount of surfactant[6,7].

The study of the formation of microporous polymeric materials by polymerization of bicontinuous microemulsions has attracted much interest recently[8–15]. The so prepared microporous polymeric materials may find potential applications in the separation technology. It is well known that the performance of a composite membrane depends on its microstructure for its selectivity, flux and rejection. Many ways are available for membrane design. For polymer membranes, the formation of solid films can be achieved by precipitation or phase inversion from polymer solutions[16,17], and polymerization of concentrated emulsion[18,19]. However, a precise regulation of the pore size of membranes is not easy because even a slight fluctuation of the processing conditions might cause a broad pore size distribution.

In our recent studies[14,15], we have found that the polymerization of bicontinuous microemulsions using sodium dodecyl sulfate (SDS) and *n*-dodecyltrimethyl ammonium bromide (DTAB) leads to the formation of interconnected globular network via the coagulation mechanism. The pores or voids were the water-filled spaces between the incompletely coalesced spherical aggregates. It has also been shown[10–12,14,15] that polymerization of w/o- and bicontinuous microemulsions will lead to the formation of closed-cell and open-cell structures respectively.

* To whom correspondence should be addressed

In this work, the phase behaviour of methyl methacrylate (MMA), 2-hydroxyethyl methacrylate (HEMA), water and cationic surfactant of *n*-alkyl trimethyl ammonium bromide of varying chain-lengths was studied. Monomer HEMA acts as a cosurfactant before polymerization. A cross-linker, ethylene glycol dimethacrylate (EGDMA) was also added to serve two purposes. Firstly, it increases the mechanical strength of the polymeric materials formed. Secondly, it helps to shorten the gelation time. The effect of alkyl chain lengths of the cationic surfactant on the microstructures of the polymeric materials by microemulsion polymerization will be discussed in this paper.

EXPERIMENTAL

Materials

Methyl methacrylate (MMA) from BDH and both 2-hydroxyethyl methacrylate (HEMA) and ethylene glycol dimethacrylate (EGDMA) from Merck were purified under reduced pressure to remove inhibitor before use. Dibenzyl ketone (DBK) of purity >98% was used as received from TCI. All dodecyl trimethylammonium bromide (C_{12}TAB), tetradecyl trimethyl ammonium bromide (C_{14}TAB) and cetyl trimethylammonium bromide (C_{16}TAB) from TCI of purity >98% were recrystallized from acetone–ethanol mixture (3 : 1, v/v) before use. Millipore water of conductivity approximately 1.0 μS cm^{-1} was used.

Phase behaviour of microemulsion systems

The transparent regions of the microemulsion systems consisting of MMA, HEMA, water and *n*-alkyl trimethyl ammonium bromide of varying chain length (C_nTAB) were determined visually at room temperature (30°C). EGDMA added was 4 wt% based on the total weight of MMA and HEMA used for all the systems. Aqueous solutions containing 20 wt% C_{12}TAB, C_{14}TAB or C_{16}TAB each were prepared. Titrations of each aqueous solution of surfactant to a series of mixtures of different proportions of MMA, HEMA and EGDMA were done in culture tubes with screw caps. Viscosity measurements for each system were carried out using Cannon (USA) calibrated Ubbelohde Dilution Viscosmeter (size-100), while an Omega CM-155 Conductivity Meter with a cell constant of 1.0291 cm^{-1} was used to determine their conductivities.

Microemulsion polymerization

Prior to polymerization, microemulsion samples were transferred into glass ampoules, purged with nitrogen gas and then sealed. The photoinitiator (DBK) of 0.3 wt% based on the total weight of each microemulsion sample was used to initiate the polymerization. Each sample was then irradiated with u.v. light for a duration of 2 h at 35°C ± 0.5°C. All the polymer samples used for the following characterization studies were prewashed several times with hot water at 50°C till free of surfactant as confirmed by the elemental analysis except those for determining the drying rate of water desorption.

Electron microscopic investigation

A Hitachi S-4100 Field Emission Scanning Electron Microscope (FESEM) was used to examine the morphology of the resulting solid polymeric materials. The samples were freeze-fractured mechanically and vacuum dried at room temperature for 24 h before coating with gold using a JEOL ion-sputter JFC-1100 coating machine.

Thermal analysis

(a) Drying rate of water desorption. The drying rate of water desorption from the polymerized samples was monitored using a Dupont Instruments TGA 2960 thermogravimetric analyser. The polymer sample was dried in a stream of dry nitrogen gas isothermally at 75°C for 5 h, before a temperature ramp of 2°C min^{-1} was applied until 100°C followed by keeping at this temperature for 1 h in order to obtain the final weight of the polymer which was free from any moisture. Detailed descriptions of the determination have been published elsewhere[12].

(b) Glass transition temperature. The glass transition temperature (T_g) of the polymers which had been pretreated with hot water as mentioned above were measured using a Dupont DSC2920 Differential Scanning Calorimeter with a heating rate of 10°C min^{-1}. The initial onset of the slope of the d.s.c. curve was taken as T_g.

(c) Thermoporometry. A Dupont Instruments DSC2920 Differential Scanning Calorimeter along with a Dupont Thermal Analyst 2210 System and Liquid Nitrogen Cooling Accessory (LCNA) was used to measure and analyse the endothermic heat effects of the polymer samples during the melting of ice in the pores. About 10–20 mg of the water-saturated polymer sample which had been pretreated similarly as those used for glass transition temperature determination, was hermetically sealed in a high-pressure sample pan. The sample was placed in dry ice for 24 h in order to ensure complete freezing. The sample was further cooled to −40°C before a temperature ramp of 0.5°C min^{-1} was applied until 10°C. This low rate of heating was used to avoid kinetic effects. Pore volume distribution curve was obtained by analysing the d.s.c. thermogram in accordance with the thermoporometry method described by Brun *et al.*[20].

According to Brun *et al.*[20], the amount of undercooling ΔT for water with $0 > \Delta T > -40$ is related to the radius r of the pores by

$$r = \frac{-32.33}{\Delta T} + 0.68 \qquad (1)$$

and the apparent energy of melting, W_a, which is also a function of undercooling, ΔT, is given by:

$$W_a = -0.155\Delta T^2 - 11.39\Delta T - 332 \qquad (2)$$

The pore volume distribution dV/dr evaluated from the d.s.c. thermogram obtained during the melting of ice in the pores is given by[21]:

$$\frac{dV}{dr} = \frac{\Delta T}{32.33\rho W_a} \frac{q}{d\Delta T/dt} \qquad (3)$$

where ρ is the water density corresponding to ΔT, W_a the apparent energy of melting and q, measured by d.s.c., is the heat flux required for the melting.

Swelling equilibrium

The pretreated polymer sample was cut into small pieces and then dried to a constant weight in a vacuum oven at room temperature. The polymer pieces were then swelled in water at 30°C until they reached equilibrium and their gains in weight were recorded. The equilibrium water content (EWC) expressed as a percentage is given by

$$\mathrm{EWC}(\%) = \frac{W_s - W}{W_s} \times 100 \qquad (4)$$

where W_s and W refer to the weight of the swollen polymer sample at equilibrium swelling and the dried polymer sample respectively.

RESULTS

Characterization of microemulsion systems

Figure 1 shows the phase diagram of the systems MMA/HEMA/C_nTAB/water. The number of carbon, n, of the alkyl chain length of C_nTAB was varied from C12 to C16. The amount of C_nTAB used for each system was maintained at 20 wt% in water. EGDMA used was always fixed at 4.0 wt% based on the total weight of MMA and HEMA. A large single-phase transparent microemulsion region extended from the water-rich apex to the HEMA-rich apex and a multi-phase region D were obtained for each system. A rough demarcation within the transparent region (A, B and C) of the phase diagram was deduced from the phase behaviour studies by conductivity and viscosity measurements. It is believed that region A represents w/o microemulsions, region B o/w microemulsions and region C bicontinuous microemulsions. At lower content of the C_nTAB aqueous solution in each system, the formation of single-phase microemulsion region seemed to be independent of the alkyl chain lengths of the cationic surfactants. On the other hand, at aqueous solution content greater than

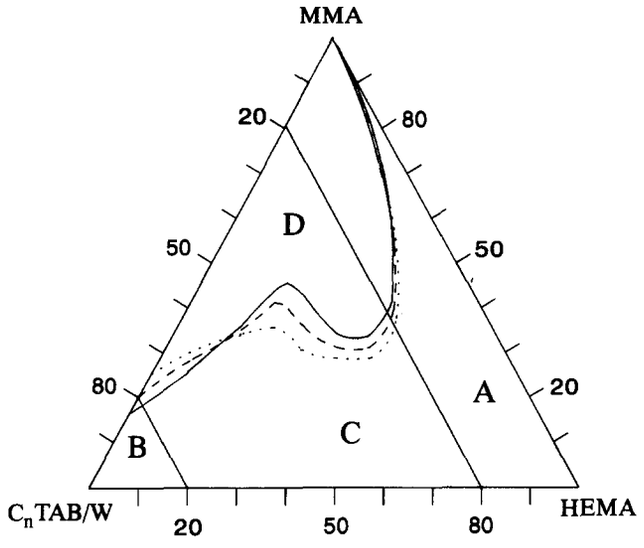

Figure 1 The phase diagram of the system MMA/HEMA/C_nTAB/water at 30°C. (——) represents the microemulsion region when $n = 12$; (– – –) for system when $n = 14$; (·····) for system when $n = 16$. EGDMA added at 4 wt% based on the total weight of monomers. The amount of C_nTAB in each system was fixed at 20 wt% in water. Domains: A, w/o microemulsion; B, o/w microemulsion; C, bicontinuous microemulsion; and D, multiphase region

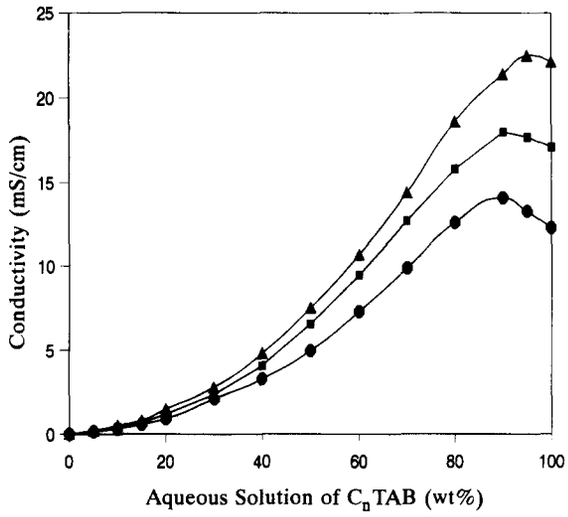

Figure 2 The conductivity curves plotted as a function of aqueous solution of *n*-alkyltrimethyl ammonium bromide surfactant. The amount of each surfactant used was 20 wt% in water. EGDMA added was 4.0 wt% based on the total weight of MMA and HEMA used. MMA:HEMA ratio was always maintained at 1:4. (–▲–): C_{12}TAB; (–■–): C_{14}TAB; (–●–): C_{16}TAB

60 wt%, a slightly larger single-phase microemulsion region was formed with increasing alkyl chain length of the surfactant. However, a smaller single-phase microemulsion region was formed with increasing alkyl chain length of the surfactant with the aqueous contents between 20 and 60 wt%. It should be pointed out that this phase behaviour became pronounced only when carbon number along the alkyl chain length of the cationic surfactant was equal or greater than 10 or a higher surfactant concentration was employed.

The variation of conductivity of the microemulsion systems with aqueous solution of cationic surfactants with various alkyl chain-lengths (C_nTAB) is shown in *Figure 2*. In these systems, MMA:HEMA ratio was maintained at 1:4 and C_nTAB was kept constant at 20 wt% in water. All the systems show a similar trend of low conductivity at low aqueous solution content (<20 wt%), followed by a rapid increase in conductivity at the aqueous solution content greater than 20 wt% and finally a small decrease in conductivity beyond 90 wt% aqueous solution. Although the amount of cationic surfactants used in each system was expressed in weight percent (wt%) and thus their concentrations in mol dm^{-3} were somewhat different, it may still be concluded that the conductivity of the system using C_{12}TAB exhibited a higher conductivity as compared to those using C_{14}TAB and C_{16}TAB. For example, the maximum conductivity of 20 wt% C_{12}TAB (22.1 mS cm^{-1}) was *ca.* 2 times higher than that of C_{16}TAB (12.2 mS cm^{-1}), while their concentrations (in terms of mol dm^{-3}) of C_{12}TAB was only *ca.* 1.2 times higher than that of C_{16}TAB.

Figure 3 shows the change in viscosity *versus* aqueous solution of C_nTAB with compositions identical to those used for the conductivity measurements as shown in *Figure 2*. The increase in viscosity was quite similar for all the three microemulsion systems containing less than 20 wt% aqueous solution. As the aqueous solution content increased beyond 20 wt%, the viscosity of the C_{12}TAB system remained almost constant up to about 90 wt% and then decreased. The viscosity remained

Table 1 Bicontinuous microemulsion compositions used for polymerization[a]

Microemulsion systems	Type of surfactant	Compositions (wt%)				Appearance[b]	
		Surfactant	Water	MMA	HEMA	BD	AD
D10	C_{12}TAB	10	40	10	40	BY	C
T10	C_{14}TAB	10	40	10	40	WY	Tl
C10	C_{16}TAB	10	40	10	40	WY	Tl

[a] Weight ratio of MMA : HEMA was fixed at 1 : 4. Cationic surfactant in water was maintained at 20 wt%. EGDMA added was 4 wt% based on the total weight of MMA and HEMA, and photoinitiator DBK added was 0.3 wt% based on the total weight of each microemulsion sample
[b] BD = before drying; AD = after drying; WY = white yellowish; BY = bluish yellow; Tl = translucent; C = clear

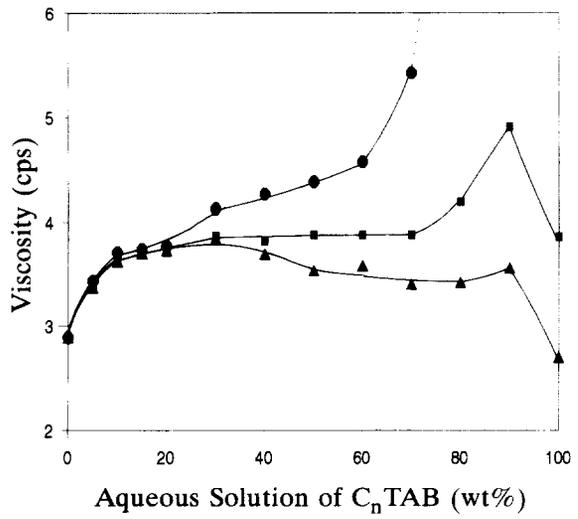

Figure 3 The viscosity curves plotted as a function of aqueous solution of *n*-alkyltrimethyl ammonium bromide surfactant. The amount of each surfactant used was 20 wt% in water. EGDMA added was 4.0 wt% based on the total weight of MMA and HEMA used. MMA : HEMA ratio was always maintained at 1 : 4. (–▲–): C_{12}TAB; (–■–): C_{14}TAB; (–●–): C_{16}TAB

almost constant up to about 70 wt% aqueous solution for the system employing C_{14}TAB, before it increased slightly and then decreased. This is in contrast to the system employing C_{16}TAB where the viscosity increased continuously up to about 60 wt% aqueous solution and it showed a sharp increase in the viscosity thereafter.

Polymerizations

Table 1 lists the bicontinuous microemulsion compositions used for the polymerization study. The polymerization was photoinitiated by 0.3 wt% DBK based on the total weight of each microemulsion sample. The polymerization proceeded very rapidly and formed a clear soft gel within 10 min. The clear soft gel slowly changed to bluish yellow or white yellowish on further polymerization dependent on the alkyl chain length of surfactant. The opacity of the polymeric materials decreased with the decrease in the alkyl chain length of surfactant. However, these bluish-yellow and white-yellowish polymeric materials changed to clear and slightly translucent in appearance respectively after drying them in an oven at 100°C for 30 min.

Microstructure of polymeric materials

The alkyl chain length of cationic surfactants (C_nTAB) shows a marked effect on the morphology of the polymeric materials as depicted in *Figures 4*, *5* and *6*

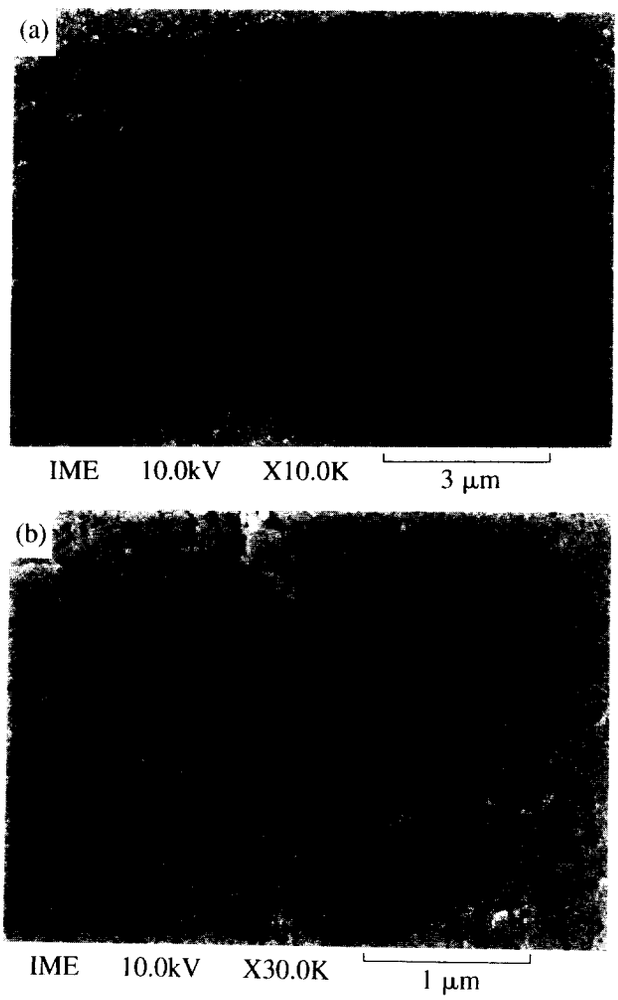

Figure 4 FESEM micrographs of the porous polymer sample D10 of compositions shown in *Table 1*. (a) Surface in direct contact with the glass wall of ampoule, (b) fractured surface.

for polymer samples D10, T10 and C10 respectively. *Figures 4a*, *5a* and *6a* show the morphology of the polymer samples in direct contact with the glass wall of ampoules, while *Figures 4b*, *5b* and *6b* show their corresponding fractured surfaces. Some deformation during the fracturing process can also be seen from the micrographs for the fractured surfaces. Globular structures were observed in polymer sample D10 prepared from the precursor microemulsion containing C_{12}TAB as shown in *Figure 4a*. The globular structures range from *ca.* 20 to 200 nm. In addition, the size of pores/voids can be seen from *Figure 4b* to be in the range of 20–100 nm. On increasing the alkyl chain length of the

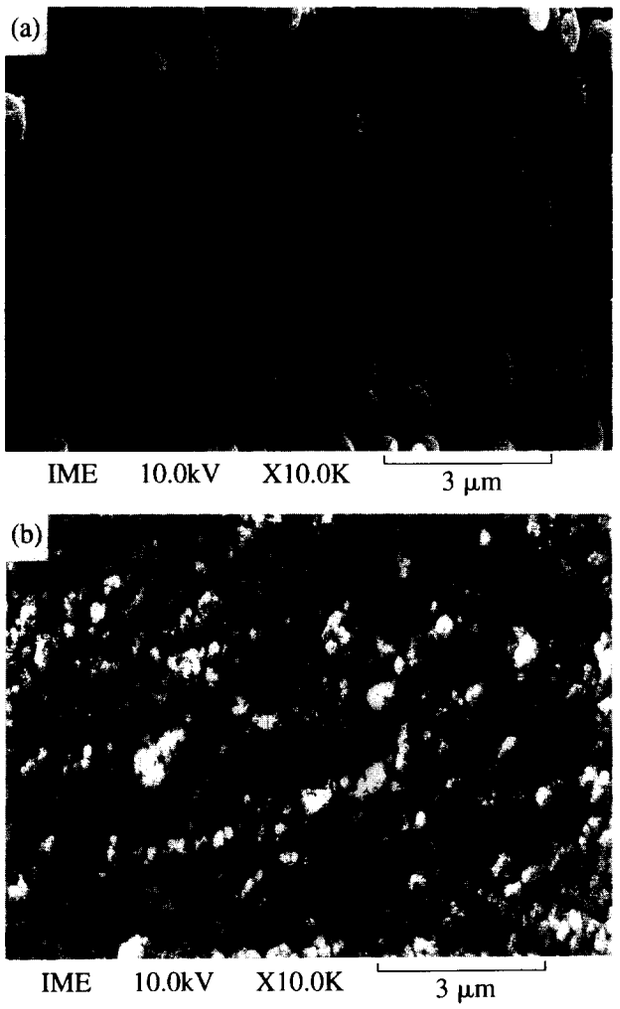

Figure 5 FESEM micrographs of the porous polymer sample T10 of compositions shown in *Table 1*. (a) Surface in direct contact with the glass wall of ampoule, (b) fractured surface

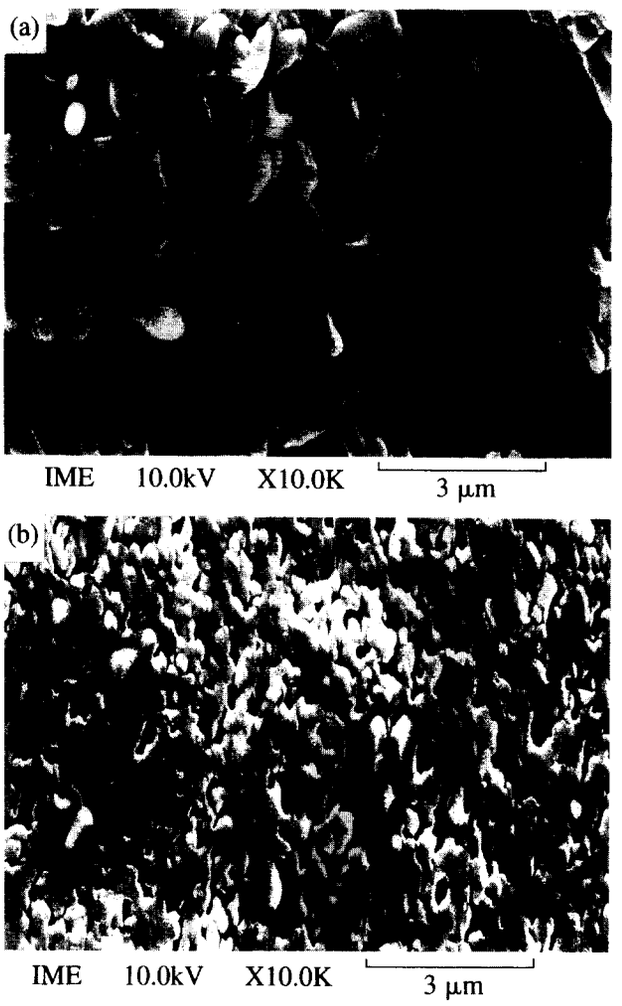

Figure 6 FESEM micrograph of the porous polymer sample C10 of compositions shown in *Table 1*. (a) Surface in direct contact with the glass wall of ampoule, (b) fractured surface

surfactant to 14 (polymer sample T10), the oval-shaped microstructures as seen from *Figure 6a* were very different from that of sample D10. They were *ca.* 0.4–1.0 μm in length and 0.2–0.5 μm in diameter. The pores/voids as observed for the fractured polymer surface of *Figure 5b* were *ca.* 20–300 nm. When C_{16}TAB was used for sample C10, elongated and worm-like structures can be clearly seen from *Figure 6*. The structures were *ca.* 1–2 μm in length and *ca.* 0.2–0.5 μm in diameter and their pore sizes as observed in *Figure 6b* were *ca.* 20–1000 nm. All the pores/voids in the polymer samples D10, T10 and C10 were believed to be water-filled spaces between incompletely coalesced aggregates of the microstructures.

Thermal analysis

All polymer samples D10, T10 and C10 show an initial linear falling rate period followed by an exponential decay, a behaviour typical of porous open-cell structures[22,23]. *Figure 7* depicts the drying rate curves of polymer samples D10 and C10. The drying rate increased on increasing the alkyl chain length of the surfactant.

Figure 8 shows the thermograms for polymer samples C10, T10 and D10. Equations (1)–(3) used for the analysis of thermograms are based on the assumption of

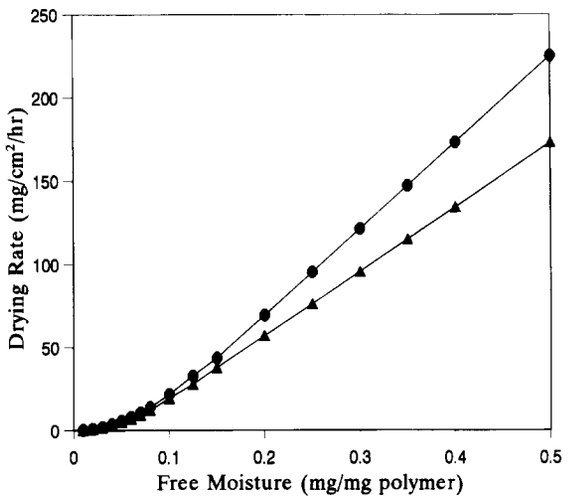

Figure 7 The drying rate curves for polymer sample C10 (–●–) and D10 (–▲–)

solid–liquid thermodynamic equilibrium. It has been reported[24] that the scanning rate less than 3°C min^{-1} performed well under equilibrium conditions, therefore polymer samples were characterized with a scanning rate of 0.5°C min^{-1}. This is because if the change of

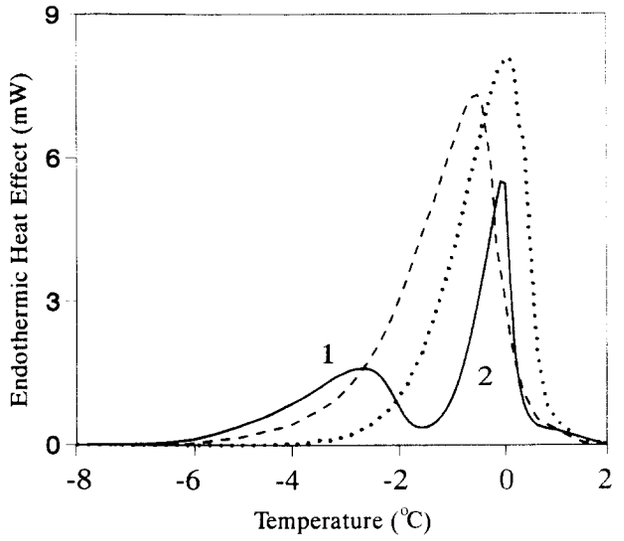

Figure 8 D.s.c. thermograms for the polymer samples D10 (——), T10 (– – –) and C10 (·····)

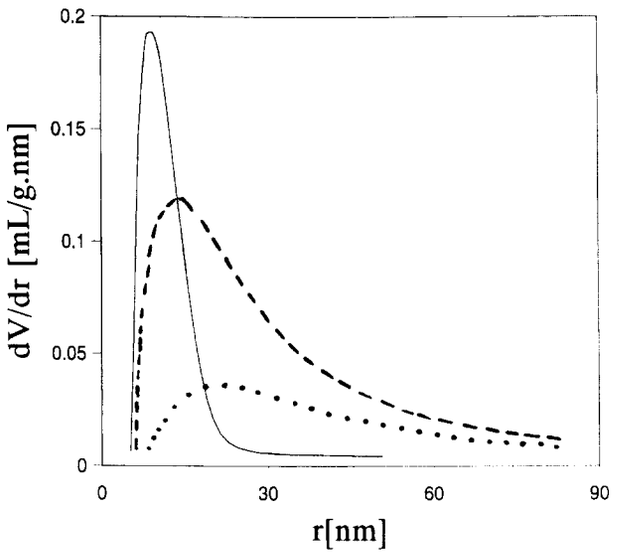

Figure 9 Pore volume distribution curves for polymer samples D10 (——), T10 (– – –) and C10 (·····)

temperature is too rapid, there exists the difficulty in detecting the melting of ice in very small pores. Two well-separated melting peaks were observed for polymer sample D10. Peak 1 represents the melting of ice in the pores of the polymer sample. Peak 2, which started at approx. 0°C, was due to the melting of ice which was not in the pores but adhered to the wall of the polymer[24]. Both samples T10 and C10 show a single broad melting peak. Similar thermograms were obtained when the samples were analysed for a second run. Subsequently, the result taken for each polymer sample was based on the first run. The peak melting temperature decreased from −2.6°C for sample D10 to −0.6°C and −0.05°C for samples T10 and C10 respectively. The lowest melting temperatures taken as the point whereby the heat flow deviated from the baseline for sample D10 was −7.0°C while that of samples T10 and C10 were −5.4 and −3.5°C respectively. The analysis of the thermograms yielded pore volume distribution curves as shown in

Table 2 Glass transitions temperature (T_g) of polymers by photo-initiated polymerization

Polymers[a]	T_g (°C)
PMMA	97
PHEMA	94
HM	95
C10	113
T10	113
D10	112

[a] HM: copolymer of MMA and HEMA crosslinked with 4.0 wt% EGDMA with weight ratio of MMA:HEMA fixed at 1:4. PMMA: poly(methyl methacrylate); PHEMA: poly(2-hydroxyethyl methacrylate); polymer samples C10, T10, and D10 have compositions shown in *Table 1*. DBK added was 0.3 wt% based on total weight of each sample. PMMA, PHEMA and HM were prepared by bulk photoinitiated polymerization

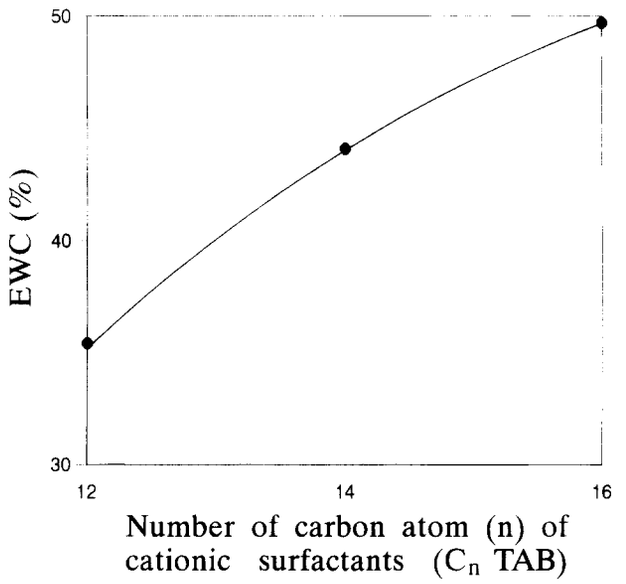

Figure 10 The equilibrium water content (EWC) for the polymers as a function of alkyl chain length of *n*-alkyltrimethyl ammonium bromide surfactant (C_nTAB)

Figure 9. A narrower distribution of pore size was observed for polymer sample D10 as compared to those of samples T10 and C10, with the maxima increasing in the order of C10, T10 and D10. Pore distributions were found to be in the range 5–20 nm for D10, 5–50 nm for T10 and 10–100 nm for C10.

The glass transition temperatures (T_g) of the polymer samples are listed in *Table 2*. The T_g for poly(methyl methacrylate) (PMMA) and poly(2-hydroxyethyl methacrylate) (PHEMA) prepared by photoinitiated bulk polymerization were 97 and 94°C respectively. T_g for the copolymers (PMMA-*co*-PHEMA) with MMA:HEMA ratio of 1:4, cross-linked with 4.0 wt% EGDMA was determined to be 95°C. It is noted that the T_g values for polymers prepared from bicontinuous microemulsion polymerization were higher (~112°C) than their respective copolymers prepared by bulk polymerization. But no particular trend in the change of T_g was observed when the alkyl chain length of the surfactant was increased from C12 to C16. The increase in T_g for polymer samples prepared from bicontinuous microemulsions may be due to the existence of different microenvironments which lead to the formation of

different copolymer microstructures as compared to that prepared by bulk polymerization. It has been reported[25,26] that microemulsion polymerization process yields copolymers with more homogeneous in composition as compared to that obtained by solution polymerization.

Swelling equilibrium

The equilibrium water content (EWC) obtained for polymer samples was plotted against the alkyl chain length of cationic surfactants (n) used in the microemulsion systems and the results are shown in *Figure 10*. The EWC increased almost linearly on increasing the values of n indicating the increase of the pore size of the polymeric materials.

DISCUSSION

Microemulsion characterization

A large microemulsion region extended from the water-rich apex to the oil-rich apex was obtained for each system under study. This is mainly due to the presence of HEMA which acts as a cosurfactant and has the effect of increasing the flexibility and fluidity of the interfacial film. Robins[27] defines a hydrophilic–lipophilic (H/L) ratio which relates the size and water solubility of a surfactant polar head (the hydrophilic) to the size and oil solubility of a hydrocarbon tail (the lipophilic). The longer the hydrocarbon chain of a surfactant, the smaller is the H/L ratio which favours the formation of larger microemulsion droplets with higher oil solubilizations. This explains why a larger single-phase microemulsion region was obtained on increasing the alkyl chain lengths of the surfactants when the water content of the microemulsions was greater than 50 wt% as shown in *Figure 1*. However, no appreciable change in the formation of single-phase microemulsion is noted for the w/o microemulsion on increasing the alkyl chain lengths of the surfactants. Since a homologue series of C_nTAB which consists of an identical head group was employed, a change in alkyl chain length of surfactant will affect mainly on the surfactant packing characteristics[28], and its specific interaction with oils[29] while leaving the head group region of the surfactant intact and preserving the desirable characteristics of the system. As a result, alkyl chain length of surfactant has no significant influence on the formation of single-phase region in w/o microemulsions. In the bicontinuous microemulsion region with the water content in between 20 and 50 wt%, a smaller transparent region was formed for a surfactant with a longer chain-length as compared to that with a shorter chain-length. This may be due to the fact that a longer surfactant chain-length is more densely packed at the interface to form a thicker interfacial layer. The formation of a more rigid surfactant monolayer, thus harder to bend, is unfavourable for the formation of bicontinuous microemulsions[30,31]. De Gennes and Taupin[32] predicted that very low rigidity of the surfactant layer is required for producing a bicontinuous microemulsion.

The conductivity behaviour for the systems investigated was due to the transformation of w/o microemulsion droplets at lower aqueous content (<20 wt%), to o/w microemulsion droplets at higher aqueous content (>90 wt%) through the intermediate bicontinuous structures as has also been reported in the literature[33–35]. The higher conductivity exhibited by system $C_{12}TAB$ compared to that of $C_{14}TAB$ and $C_{16}TAB$ was due to the higher solubility of $C_{12}TAB$ in water than the others.

The viscosity results provide some information regarding the interactions between water (or oil) droplets/domains and thus the microstructures of a microemulsion. With droplet structures as for especially w/o microemulsions, their viscosities were relatively low. But the viscosities for bicontinuous structures were higher than those of droplet structures due to their interconnections. From the information of conductivity and viscosity, it is believed that bicontinuous microemulsions were formed in region C containing 20–90 wt% aqueous solution of C_nTAB as shown in *Figure 1*. An abrupt increase in viscosity was observed for the system $C_{16}TAB$ when aqueous solution content >60 wt%. This was due to the formation of rod-like micellar structures for $C_{16}TAB$ at higher concentration as reported in the literature[36,37].

Bicontinuous microemulsion polymerizations

It is known that MMA, HEMA and EGDMA can be easily copolymerized with each other to form a cross-linked terpolymer. A fast rate of polymerization at a relatively low temperature may be required though not so critical to alleviate the occurrence of phase separation. Once the polymerization starts, the initial bicontinuous structures may break up due to the increase in the interfacial tension. This is because the oil–water interfaces of the bicontinuous microemulsions are flexible and fluctuating and they can easily undergo deformations. In our recent study[38] on the polymerization of bicontinuous microemulsions for the system consisting of MMA/HEMA/sodium dodecyl sulfate (SDS)/water, the polymerization starts with the generation of spherical polymer particles as examined under transmission electron microscope. The results indicate that the bicontinuous structures cannot be preserved under polymerization. This is substantiated by the final morphology observation which shows the formation of interconnected globular, oval-shaped and elongated structures as observed from FESEM micrographs. The mechanism for forming these structures is still under investigation.

Characterization of polymeric materials

The prominent changes in the microstructure on increasing the alkyl chain length of surfactant may be related to the stabilization of the growing polymer particles. A surfactant with longer chain length may be more effectively anchored to the polymer surfaces due to greater hydrophobic interactions. Thus the rate of mutual coagulation between polymer particles is reduced. Hence, these polymer particles can grow to bigger sizes before the coagulation occurs. On the other hand, a shorter surfactant chain-length is less effective in preventing the coagulation with the neighbouring particles before the polymer particles can grow to larger sizes. Thus smaller globular structures were observed for the system using a shorter chain-length surfactant. This also explained why the opacity of the polymers decreases on decreasing the chain length of surfactant. However, it is not well understood about the

transformation of the polymer structures from globular to worm-like shape on increasing the alkyl chain length of the surfactant. It seems to be associated with the rigidity and packing of the surfactant at the interface. A shorter surfactant chain-length will give rise to a more flexible interfacial film which is easier to bend and thus lead to the formation of globular structures. On the contrary, a longer surfactant chain-length may form a more rigid interfacial film resulting in the formation of elongated worm-like structures. In addition, some nucleation of polymer particles may also occur in the aqueous phase during the process of polymerization. This is due to the presence of water-soluble HEMA and partially water-soluble MMA. As a result, surfactants are required to stabilize these polymer particles. It is believed that those polymer particles generated in the aqueous phase will form spherical particles. This may account for the observation of both worm-like and spherical aggregates for polymer sample C10 as depicted in *Figure 6*.

Based on the shape of the drying rate curve obtained, a distinction can be made between open-cell and closed-cell structures in the polymeric materials[20,21]. It is known that solid materials having the closed-cell structure will exhibit a drying rate curve which has an exponential falling rate period whereas that with the open-cell structure has a linear falling rate period as revealed in *Figure 7*. In porous solids, the moisture flows through capillary action. As water is removed by vaporization, a meniscus across each pore is formed, which sets up capillary forces by the interfacial tension between the water and the solid. The strength of capillary forces at a given point is a function of the pore cross section. As water is progressively depleted, the linear falling rate period reaches a critical point into which there is insufficient water left to maintain a continuous film across the pores. When this state appears, the rate of drying again decreases exponentially corresponding to diffusion of water vapour through the solid as can clearly be seen from *Figure 7* at free moisture content below 0.1 mg/mg polymer. It is thus established that polymer samples D10, T10 and C10 consisted of open-cell type structures.

A decrease in peak melting temperature in the endotherm as a function of chain length of surfactant indicates an increase in pore size with increasing chain length of a surfactant. As also evinced from FESEM micrographs and pore volume distribution curves, the pore sizes of sample D10 were much smaller than those of samples T10 and C10. This is also reflected in the slower drying rate of water for sample D10 than that for sample C10 as shown in *Figure 7*. However, the pore dimensions as determined by thermoporometry are much smaller from those observed in the FESEM micrographs. It seems that the capillary structures collapse during the drying process and thus form larger pore morphologies as has also been observed in other systems[39]. In addition, the EWC result of *Figure 10* also supports that the pore sizes of the polymeric materials increase with the increase in the alkyl chain length of surfactant.

CONCLUSIONS

A wide composition range for preparing bicontinuous microemulsions can be obtained from systems consisting of MMA/HEMA/EGDMA/water and C_nTAB of various alkyl chain lengths. Some of these bicontinuous microemulsions have been successfully polymerized to produce microporous polymeric materials with open-cell structures. The alkyl chain lengths of the cationic surfactants did significantly affect the microstructures of the final polymeric materials. The different sizes of pores as occupied by water in the polymeric materials may be formed from the coalescence of growing polymer particles during the polymerization. The present study provides some information about the possibility for controlling the microstructures of polymeric materials prepared from bicontinuous microemulsions using various alkyl chain lengths of cationic surfactants.

REFERENCES

1 Atik, S. S. and Thomas, J. K. *J. Am. Chem. Soc.* 1981, **103**, 4279
2 Antoneitti, M., Bremser, W., Muschenborn, D., Rosenauer, C., Schupp, B and Schmidt, M. *Macromolecules* 1991, **24**, 6636
3 Guo, J. S., Sudol, E. D., Vanderhoff, J. W. and El-Aasser, M. S. *J. Polym. Sci. Part A: Polym. Chem.* 1992, **30**, 691
4 Candau, F. in 'Polymerization in Organized Media' (Ed. M. Paleos), Gordon & Breach, 1992, p. 215
5 Gan, L. M., Chew, C. H., Lee, K. C. and Ng, S. C. *Polymer* 1994, **34**, 3064
6 Candau, F., Zekhnini, Z. and Durand, J. P. *J. Colloid Interface Sci.* 1986, **114**, 398
7 Holtzscherer, C. and Candau, F. *J. Colloid Interface Sci.* 1988, **125**, 97
8 Qutubuddin, S., Haque, E., Benton, W. J. and Fendler, E. J. in 'Polymer Association Structures: Microemulsion and Liquid Crystals' (Ed. M. A. El-Nokaly), ACS Symposium Series No. 384, American Chemical Society, Washington, DC, 1989, p. 64
9 Sasthav, M. and Cheung, H. M. *Langmuir* 1991, **7** 1378
10 Palani Raj, W. R., Sasthav, M. and Cheung, H. M. *Langmuir* 1991, **7**, 2586
11 Palani Raj, W. R., Sasthav, M. and Cheung, H. M. *Langmuir* 1992, **8**, 1931
12 Palani Raj, W. R., Sasthav, M. and Cheung, H. M. *J. Appl. Polym. Sci.* 1993, **47**, 499
13 Gan, L. M., Chieng, T. H., Chew, C. H. and Ng, S. C. *Langmuir* 1994, **10**, 4022
14 Chieng, T. H., Gan, L. M., Chew, C. H. and Ng, S. C. *Polymer* 1995, **36** 1941
15 Chieng, T. H., Gan, L. M., Chew, C. H., Ng, S. C., Lee, L., Pey, K. L. and Grant, D. *Langmuir* 1995, **11**, 3321
16 Kesting, R. E. in 'Synthetic Polymeric Membranes: A Structural Perspective', 2nd Edn, Wiley-Interscience, 1985, p. 237
17 Wienk, I. M., van den Boomgaard, Th. and Smolders, C. A. *J. Appl. Polym. Sci.* 1994, **53**, 1011
18 Rukenstein, E. and Sun, F. *J. Appl. Polym. Sci.* 1992, **46**, 1271
19 Rukenstein, E. and Li, H. *Polymer* 1994, **35**, 4343
20 Brun, M., Lallemand, A., Quinson, J. F. and Eyraud, C. *Thermochim. Acta* 1977, **21**, 59
21 Nakao, S. *J. Membrane Sci.* 1994, **96**, 131
22 Coulson, J. M. and Richardson, J. F. in 'Chemical Engineering', 2nd Edn, Pergamon, New York, 1968, Vol. II, p. 620
23 McCabe, W. L., Smith, J. C. and Harriot, P. in 'Unit Operations of Chemical Engineering', 4th Edn, McGraw-Hill, New York, 1985, p. 716
24 Kim, K. J., Fane, A. G., Ben Aim, R., Liu, M. G., Jonsson, G., Tessaro, I. C., Broek, A. P. and Bargeman, D. *J. Membrane Sci.* 1994, **87**, 35
25 Corpart, J. M., Selb, J. and Candau, F. *Polymer* 1993, **34**, 3873
26 Candau, F., Zekhnini, Z. and Heatley, F. *Macromolecules* 1986, **19**, 1895
27 Robbins, M. L. *J. Colloid Interface Sci.* 1988, **124**, 462
28 Chen, V., Wan, G. G., Evans, D. F. and Prendergast, F. G. *J. Phys. Chem.* 1988, **3**, 92
29 Gruen, D. W. R. and Haydon, D. A. *Pure Appl. Chem.* 1980, **52**, 1229

30 Lee, L. T., Langevin, D., Wong, K. and Abillon, O. *J. Phys.: Condens. Matter* 1990, **2**, SA333
31 Szleifer, I., Kramer, D., Ben-Shaul, A., Gelbart, W. M. and Safran, S. A. *J. Chem. Phys.* 1990, **92(11)**, 6800
32 De Gennes, P. G. and Taupin, C. *J. Phys. Chem.* 1982, **86**, 2294
33 Chen, S. J., Evans, D. F. and Ninham, B. W. *J. Phys. Chem.* 1984, **88**, 1631
34 Georges, J. and Chen, J. W. *Colloid Polym. Sci.* 1986, **264**, 896
35 Clausse, M., Zradba, A. and Nicholas-Morgantini, L. in 'Microemulsion Systems' (Eds H. L. Rosano and M. Clausse), Marcel Dekker, New York, 1987, p. 387
36 Ekwall, P., Mandell, L. and Solyom, P. *J. Colloid Interface Sci.* 1969, **29**, 639
37 Ulmius, J., Lindman, B., Lindbolm, G. and Drakenberg, T. *J. Colloid Interace Sci.* 1978, **65**, 88
38 Chieng, T. H., Gan, L. M., Chew, C. H., Ng, S. C. and Pey, K. L. *J. Appl. Polym. Sci.* in press
39 Sasthav, M., Palani Raj, W. R. and Cheung, H. M. *J. Colloid Interface Sci.* 1992, **152**, 376